metals

MDPI

Article

Oxide Scale Formation on Low-Carbon Steels in Future Reheating Conditions

Juho Haapakangas *, Sonja Riikonen, Susanna Airaksinen, Eetu-Pekka Heikkinen and Timo Fabritius

Process Metallurgy Group, University of Oulu, 90014 Oulu, Finland
* Correspondence: juho.haapakangas@oulu.fi

Abstract: The mitigation of CO_2 emissions is one of the major areas of research in iron ore-based steelmaking. In this study, four simulated current and potential future reheating scenarios with different fuel and oxidizer gases were studied regarding the amount of oxide formation and the adhesion of the steel–oxide interface: (1) methane–air; (2) coke oven gas–air; (3) hydrogen–air; (4) and an oxyfuel scenario with 50:50 methane/hydrogen as fuel gases. Isothermal oxidation tests were conducted at temperatures of 1150, 1230 and 1300 °C. Four low-carbon steel grades were tested in the previously mentioned gas atmospheres. The structure and composition of the formed oxide scales was analyzed with FESEM-EDS microscopy. The amount of oxide formation correlated with the water vapor content of the gas atmosphere for all four steel grades; however, notable differences were found between individual steel grades regarding the degree of oxidation increase. No clear evidence was found of the gas atmospheres affecting the adhesion of oxide scales to the steel substrate. The adhesion of the interface was mainly determined by the content of silicon in the steel grade and the test temperature.

Keywords: low carbon steel; reheating; oxidation; oxide scale; adhesion; hydrogen; CO_2 reduction

check for updates

Citation: Haapakangas, J.; Riikonen, S.; Airaksinen, S.; Heikkinen, E.-P.; Fabritius, T. Oxide Scale Formation on Low-Carbon Steels in Future Reheating Conditions. *Metals* **2024**, *14*, 189. https://doi.org/10.3390/met14020189

Academic Editor: Pablo Pérez Zubiaur

Received: 21 December 2023
Revised: 19 January 2024
Accepted: 24 January 2024
Published: 2 February 2024

Copyright: © 2024 by the authors. Licensee MDPI, Basel, Switzerland. This article is an open access article distributed under the terms and conditions of the Creative Commons Attribution (CC BY) license (https://creativecommons.org/licenses/by/4.0/).

1. Introduction

The Paris agreement negotiated in 2015 by 196 parties set a target to limit global warming to 1.5 °C compared to pre-industrial levels [1]. Fully decarbonizing the global industry, including the steel sector, is a part of achieving climate stabilization, and reaching net zero emissions by 2050–2070 is necessary to stay on track with the Paris Agreement [2]. In addition, the Green Deal approved in 2020 aims to make the European Union climate neutral by the year 2050. For the European steel companies to achieve such large-scale CO_2 emission targets, significant changes to the current production practices of steel must be made.

The conventional flat hot-rolling process consists of three steps, which are slab reheating, hot rolling and coiling [3]. During reheating, steel slabs are heated to temperatures of 1000–1250 °C by the combustion of a gaseous fuel. Natural gas is the most widely utilized fuel gas in reheating furnaces, but other industrial gases such as blast furnace gas or coke oven gas are also used. Air has been traditionally used as the oxidizer gas in reheating furnaces. For safety and heating efficiency consideration, excess air is generally used in combustion, which results in a free oxygen content of 1–4 % in the combustion product.

Because of the oxidizing nature of the atmosphere and the holding time of around two hours, a several millimeter thick oxide scale forms on the slab surface during reheating. This oxide is called primary scale and it is removed by a hydraulic descaler near the exit of the furnace. Understanding and controlling scale formation is of economic importance, because oxidation losses equal to 1–2% of the original metal [4]. Also, a highly adhesive metal–oxide interface can lead to insufficient descaling and cause surface defects, such as red scale formation, during the hot-rolling process [5].

Because the traditionally used fuel gases are fossil-based, the reheating of slabs is a significant source of CO_2 emissions. Due to the set CO_2 reduction targets, hydrogen is drawing more and more interest as a carbon replacement both as a reducing agent and as a source of energy. Among other potential targets, hydrogen has also been proposed as an alternative fuel to be used in reheating furnaces.

Another advancement in improving furnace efficiency is the oxyfuel process, i.e., using pure oxygen as the oxidizer gas. When air is used as the oxidizer, large amounts of energy are lost in the heating of nitrogen. In CFD simulations, oxyfuel has improved furnace efficiency [6]. It has been calculated that oxyfuel burners can reduce fuel consumption by around 16% and reduce reheating time by 6% [7].

However, the production of both hydrogen and oxygen demand large amounts of electricity. Therefore, their utilization does not automatically reduce systemwide CO_2 emissions, but is largely dependent on the amount of CO_2 emissions formed during the production of the required electricity [8].

The utilization of these new technologies will lead to large-scale changes in the gas atmospheres in reheating furnaces, especially the increased proportion of water vapor. Previous research on the effects of water vapor on the oxidation of steel has been summarized by Saunders [9]. The oxidation kinetics of steel in water vapor-containing atmospheres have been studied previously [10–18]. Rahmel and Tobolski [10] found no effects from water vapor (2–69%) on the oxidation rate at 750 °C, but at 950 °C with the highest concentration of water, the oxidation rate was increased by a factor of 1.6.

In has been shown that the presence of water vapor increases the oxidation rates of both iron and steel. It has also been reported that the plasticity and adhesion of the oxide scale are increased in moist atmospheres compared to those formed in dry conditions [11,13]. This is believed to be caused by the increased inward flux of the oxidant in moist atmospheres [9].

In previous studies, water vapor has been shown to influence the morphology of formed iron oxides. Water vapor promotes the formation of a more porous scale, which is related to an increase in cation diffusion [9]. However, more research is needed to understand how the oxidation process of steel is affected by large-scale changes in industrial reheating furnaces.

The object of this research was to conduct a laboratory-scale case study on scale formation during slab reheating when utilizing both hydrogen as the fuel source and pure oxygen as the oxidizer gas. These potential future reheating atmospheres were compared against the currently used practices of natural gas and coke oven gas. The oxidation tests were conducted using a thermogravimetric analyzer and four low-carbon steel grades were selected for the study. The scale morphology was analyzed using FESEM-EDS electron microscopy. The effects of the gas atmosphere on the oxidation rate, scale adhesion and scale morphology are discussed.

2. Materials and Methods

The thermal gravimetric analyzer (TGA) used for the oxidation tests is a custom-made vertical tubular furnace with an inner dimension of 28.5 mm. It can hold a maximum temperature of 1500 °C and utilize gases such as N_2, CO, CO_2, H_2, O_2 and H_2O. Deionized water was provided to the furnace with a peristaltic pump directly to the gas line, which was heated to around 300 °C to vaporize the water and avoid condensation. The peristaltic pump was calibrated before each test by pumping water for a specific time into a beaker glass and weighing the mass of water. The total gas flow rate in the experiments was 2 L min^{-1}. The layout of the furnace has been presented in a previous study [19].

Four simulated current and potential future reheating scenarios with different fuel and oxidizer gases were selected for this study: (1) methane–air; (2) coke oven gas–air; (3) hydrogen–air; (4) methane–hydrogen (50:50) mixture–oxygen. Methane was chosen to represent the typical industrial scenario of natural gas burn, because it is the main component of natural gas, while natural gas is the most widely utilized gas in reheating

furnaces. The composition of natural gas varies depending on its location of extraction, but it typically contains around 85% or more methane [20].

Coke oven gas is another currently utilized reheating gas, which contains slightly more hydrogen compared to natural gas. The simulated coke oven gas atmosphere was only used for steel grades A and C. Hydrogen–air highlights the changes occurring when reheating is conducted in a fossil-free scenario. CH_4–H_2–oxy was chosen as an example of a potential future scenario where methane has been partially replaced with hydrogen, and pure oxygen (oxyfuel) is used as the oxidizer gas. The compositions of the gas profiles are presented in Table 1.

Table 1. Compositions of the simulated reheating gas atmospheres used in the experiments.

Abbreviation	Fuel Gas	Oxidant	N_2	CO_2	H_2O	O_2
1. CH_4–air	Methane (CH_4)	Air	72.60	8.05	16.10	3.22
2. COG–air	Coke oven gas (COG)	Air	70.50	6.13	20.50	2.82
3. H_2–air	Hydrogen (H_2)	Air	67.20	-	29.80	3.00
4. CH_4–H_2–oxy	50% CH_4–50% H_2	Oxygen (O_2)	-	19.36	77.42	3.22

The samples were cut into rectangular shapes with dimensions of 12 × 12 × 30 mm, with minor variations between samples. After cutting, the samples were polished with SiC 220 grit paper and cleaned with ethanol. Prior to the tests, the length of all three sides of the samples was measured with a digital caliper from three different locations. The average of the three measurements was used to calculate the sample surface area.

A 2.5 mm hole was drilled in the top part of each sample for wire suspension. Through this hole, a platinum/rhodium wire was attached to a sample holder, which was then attached to a scale for continuous measurement of sample mass change.

Four different low-carbon steel grades were selected for this study. The chemical compositions of the steel grades used are provided in Table 2. Notably, steel grades B and D contained silicon, which is known to influence the oxidation rate and to increase the adhesion of the oxide scale to the steel substrate. Grade D also contains aluminum, another element known to affect the oxidation process [21,22], whereas grades A and C were mostly free of these elements. The main difference between grades A and C is in their manganese contents.

Table 2. The elemental composition of the studied low-carbon steel grades.

Steel Grade	C	Si	Mn	Nb	Al	Cr	Mo	Other	Fe
Grade A	0.12	0.01	0.2	-	0.02	0.04	0.005	-	Bal.
Grade B	0.06	0.20	1.2	0.04	0.04	0.04	0.005	V	Bal.
Grade C	0.10	0.02	1.5	0.04	0.03	0.04	0.005	Ti	Bal.
Grade D	0.11	0.36	1.7	-	<1.0	0.04	0.005	-	Bal.

Isothermal tests were conducted at temperatures of 1150, 1230 and 1300 °C. The holding time in the furnace was 200 min in each test. The samples were placed into the furnace in a gas atmosphere of 100% purified nitrogen. A pre-heating period of 5 min was included in nitrogen to allow the samples to reach the furnace temperature.

Dynamic tests were also performed to simulate the heating profile of an actual reheating furnace more accurately. The sample was introduced to the furnace at 500 °C, after which the temperature was increased to 1180 °C at a rate of 3.78 °C/min. The temperature reached its maximum point at 180 min, after which it was held for 70 min. For both isothermal and dynamic tests, the samples were taken out of the furnace and allowed to cool at room temperature in ambient air.

After the thermogravimetric tests, the samples were cold-mounted in epoxy, cross-sectioned, polished and analyzed with a field-emission scanning electron microscope (FESEM, Zeiss ULTRA plus, Oberkochen, Germany). An Oxford Instruments electron energy-dispersive X-ray (EDS) analyzer linked to the FESEM was used to identify phase composition information from the mounted samples. Backscattered electrons (BSEs) were used in the FESEM imaging.

3. Results and Discussion

3.1. Oxidation in Isothermal Conditions

The presence of water vapor alters all aspects of oxide growth, including the adsorption, dissociation and diffusion of reactants. The diffusion rate of water vapor is faster compared to oxygen. This is possible due to proton hopping, in which protons localized at oxide ions move by transfer from one oxygen to another. Because OH^- ion condensation is increased, there is a resultant increase in cation vacancies [9]. Another factor is molecular diffusion. It has been proposed [10] that when the pores and voids in the oxide contain a mixture of H_2/H_2O, oxidation occurs through water vapor at the metal–oxide side and reduction at the oxide–gas side of the pore to form water vapor. This mechanism allows for the rapid inwards diffusion of oxygen while the pore gradually moves up inside the oxide layer. These bridges enable the further oxidation of metal without substantial inhibition. However, as mentioned by Tuck [13], even when voids are not present in the oxide scale, water vapor still increases oxidation rates due to the increased plasticity of the oxide. This allows for good steel–oxide contact and uninterrupted diffusion of iron cations.

The isothermal oxidation experiments in this study were conducted using the TGA furnace previously described in Section 2. TGA tests were performed using four low-carbon steel grades and four different gas profiles at temperatures of 1150 °C, 1230 °C and 1300 °C. The surface area-adjusted weight change graphs are presented in Figure 1. The oxidation followed parabolic kinetics after a short initial linear phase.

Based on the spread of mass change curves in Figure 1, it is evident that there were large differences between the steel grades in how they were affected by changes in the gas atmosphere. To further highlight the differences between the steel grades, the increases in the total oxidation compared to the standard industrial case, CH_4–air, are presented in Table 3 in percentages. Steel grades A and D had limited increases (4.6–35.0%) in total oxidation in the future reheating scenarios of H_2–air and CH_4–H_2–oxy. On the other hand, the oxidation of grades B and C was significantly increased up to 65.1% for grade B and 90.0% for grade C. Based on the results of this study, some steel grades seem to be more sensitive to the changes in the reheating gas atmosphere than others. The reasons behind this effect are not yet clear.

Table 3. Increase in total oxidation in comparison to the CH_4–air atmosphere for different steel grades.

	Grade A			**Grade B**			**Grade C**			**Grade D**		
Temperature (°C)	1150	1230	1300	1150	1230	1300	1150	1230	1300	1150	1230	1300
CH_4–H_2–oxy	10.1%	22.2%	35.0%	39.1%	65.1%	53.3%	35.9%	74.1%	90.0%	27.1%	17.7%	18.7%
H_2–air	6.2%	14.3%	17.8%	8.2%	24.2%	24.8%	16.0%	24.8%	47.9%	15.9%	4.6%	9.1%
COG–air	0.1%	7.8%	15.3%				6.3%	7.0%	30.3%			
CH_4–air	Baseline			Baseline			Baseline			Baseline		

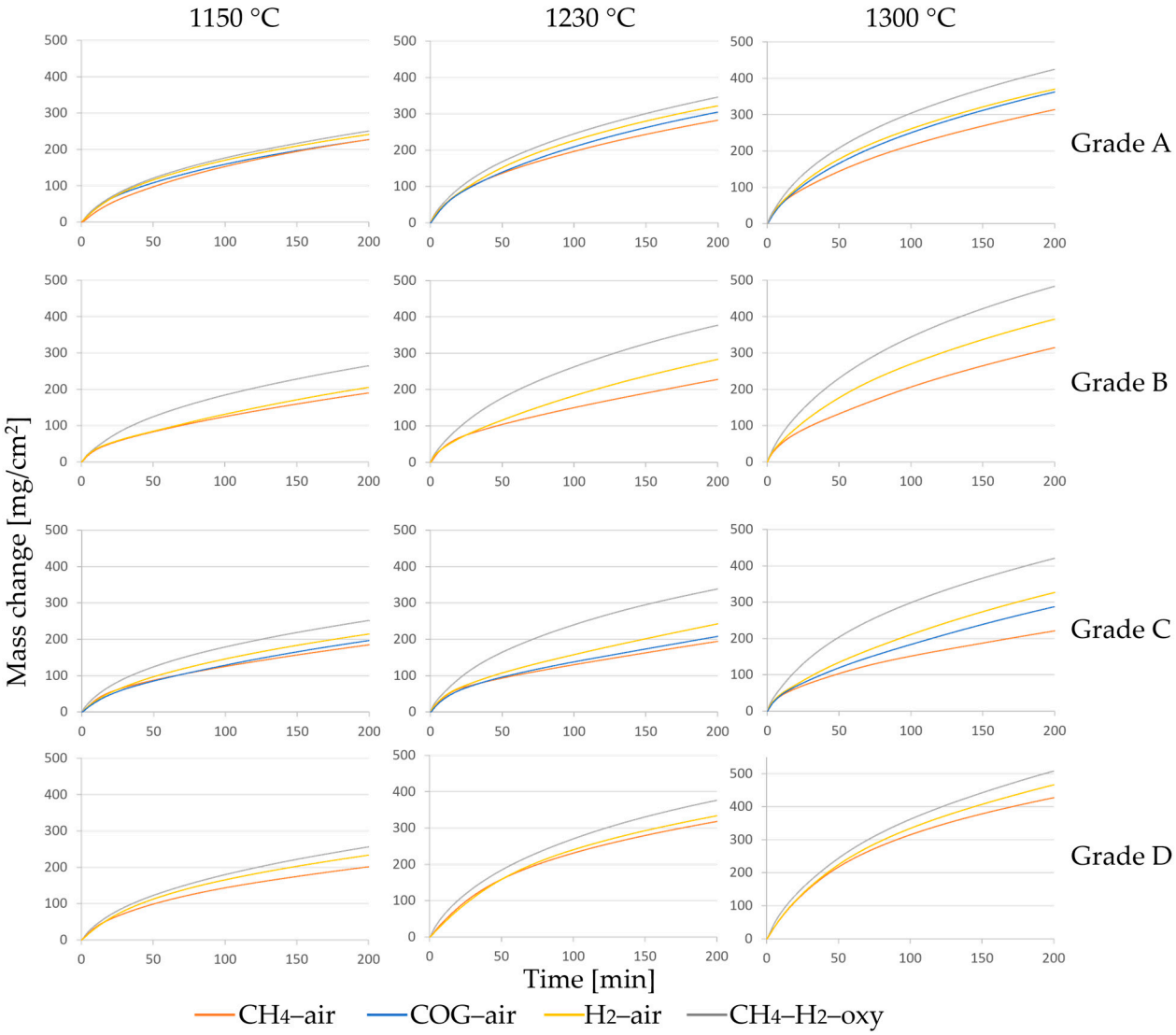

Figure 1. Mass change as a function of time in the isothermal TGA experiments.

The overall surface area-adjusted mass changes are presented in Figure 2. From Figure 2, it can be concluded that the changes in reheating temperature play a larger role for steel grades B and D, which contain more alloying elements, specifically silicon. As the heating temperature increases from 1150 °C to 1230 °C, and further to 1300 °C, the increase in oxidation is notably lower for low silicon grades (A and C) compared to grades B and D with 0.2 and 0.36% silicon, respectively.

Si in steel reacts with diffusing oxygen and forms SiO_2 below 950 °C. Between 950 °C and 1173 °C, it further combines with FeO to form fayalite (Fe_2SiO_4). In this temperature range, fayalite grains can be found inside the wüstite matrix close to the steel interface. Above the eutectic temperature of 1173 °C, a liquid phase of FeO-Fe_2SiO_4 forms, which penetrates the steel matrix and also the grain boundaries of the wüstite layer [23].

Silicon hinders the oxidation rate by acting as a diffusion barrier below the eutectic temperature; however, oxidation is rapidly accelerated above 1173 °C due to the presence of the eutectic phase [24–26]. The solidified eutectic FeO-Fe_2SiO_4 phase is mechanically strong even at only 60 °C below the liquidus temperature [5], which makes the descaling of Si-containing steels challenging.

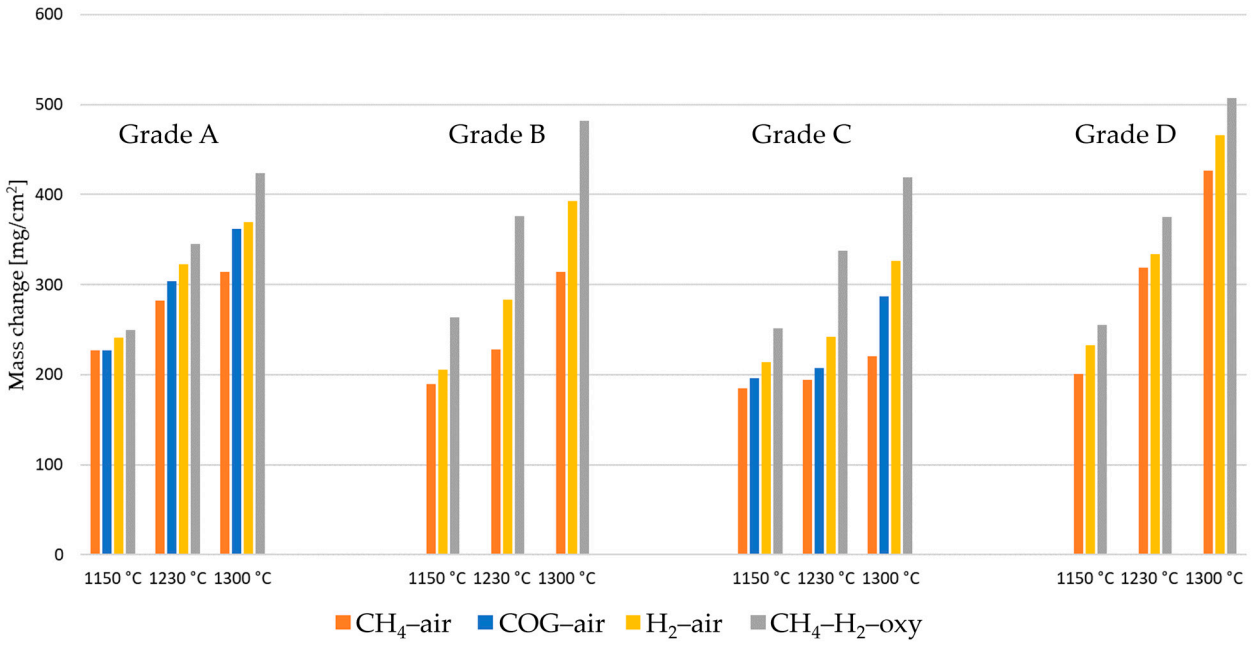

Figure 2. Total oxidation of the steel grades in different simulated combustion gas atmospheres.

The overall oxidation for all four steel grades increased in the order of:

1. CH_4–air (least oxidizing)
2. COG–air
3. H_2–air
4. CH_4–H_2–oxy (most oxidizing)

In our experiments, this order remained the same for all steel grades and in all test temperatures. This order also coincides with the water vapor content in the gas atmospheres, as highlighted in Figure 3. It is noteworthy that the CH_4–H_2–oxyfuel gas atmosphere was by far the most oxidizing gas atmosphere for all four steel grades, whereas the increase in oxidation in the carbon-free case of H_2–air was more moderate. The results indicate that regarding scaling losses, the change in the oxidizer from air to oxygen has a much higher impact when compared to the change in the fuel gas from a fossil fuel-based source to hydrogen.

Simulated gas	H_2O content in gas (vol%)	Average oxidation compared to CH_4–air		
		1150 °C	1230 °C	1300 °C
CH_4–H_2–oxy	77.4	+28.0 %	+44.8 %	+49.2 %
H_2–air	29.8	+11.6 %	+17.0 %	+24.9 %
COG–air	20.5	+3.2 %	+7.4 %	+22.8 %
CH_4–air	16.1		Baseline	

Figure 3. Relation between the H_2O content in the gas atmosphere (blue) and the increase in oxidation in comparison to the reference case CH_4–air. The percentual change highlighted in green is the calculated average value from the four steel grades.

After a 330 min oxidation test at 1230 °C, Luzzo et al. [27] found a moderate increase of 14% in total oxidation when comparing 100% H_2 to natural gas burn. The 17.0% average increase observed at 1230 °C in our experiments between H_2–air and CH_4–air is quite close to the result observed in the study mentioned above by Luzzo, although the holding time in

our experiments was notably shorter (200 min). However, as previously noted, the results between different steel grades can vary quite significantly.

The oxidation results obtained in this study indicate that if the reheating furnaces of the future are fueled with hydrogen, and especially in the case of the oxyfuel process, scaling losses will increase compared to the current practices. The scale of increase seems to vary significantly between individual steel grades.

3.2. Morphology of the Formed Oxide Scales

Field Emission Scanning Electron Microscopy (FESEM) was used to characterize the formed iron oxides. Typically, three distinct iron oxide layers could be seen. These were identified based on appearance in FESEM imagery and energy-dispersive X-ray spectroscopy (EDS) analyses. As stated by Young [4], electron microscopy can only provide semiquantitative information of oxygen content; hence, the phase composition of these layers were identified based on the previous literature, appearance and comparison of the ratios of the elements from EDS analyses.

In general, the structure of the observed iron oxide layers could be divided into three distinct layers: (1) a thick wüstite layer (light grey) closest to the steel interface; (2) magnetite precipitates mixed in wüstite (dark-grey precipitates inside a light-grey phase) in the upper part of the oxide scale; (3) a magnetite layer (dark grey) on the surface with little porosity, with typically a very thin hematite layer on the surface. The formation of magnetite precipitates in the region close to the magnetite layer occurs during the cooling phase. With most cooling rates, magnetite precipitation is essentially inevitable [28]. The general appearance of the iron oxide scales observed in this study is presented in Figure 4.

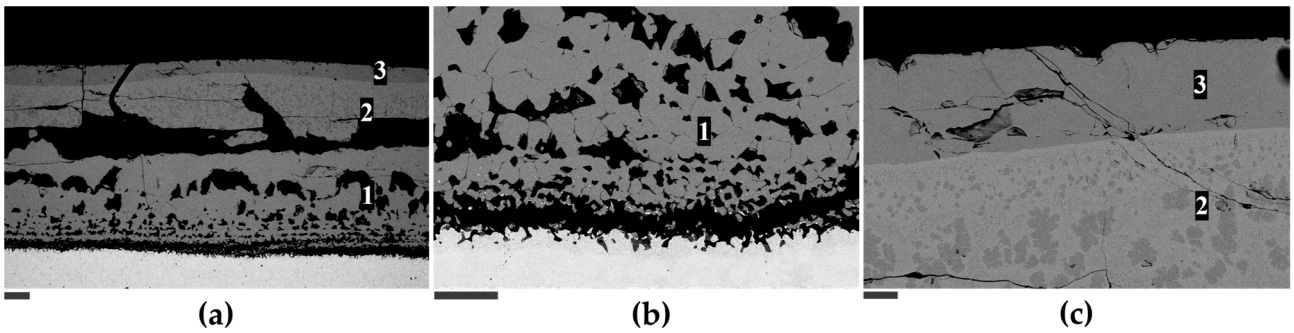

Figure 4. Oxide scale of grade B oxidized at 1150 °C in CH_4–air atmosphere. (**a**) An overview of the three-layered structure. The scale bar is 200 µm (87× magnification). (**b**) Layer 1 close to the steel substrate. The scale bar is 100 µm (428× magnification). (**c**) Layers 2 and 3 close to the oxide surface. The scale bar is 40 µm (537× magnification).

A similar oxide layer structure for steel reheated to around 1200 °C has been observed, for example, by Raman et al. [29], Yuan et al. [30] and Suarez et al. [24]. A FESEM-EDS point analysis of iron oxide layers 2 and 3 is depicted in Figure 5 and the results of the elemental point analyses are provided in Table 4.

Table 4. Results of the elemental point analyses of scale layers 2 and 3.

	S1	S2	S3	S4	S5	S6	S7	S8	S9	S10	S11	S12
Fe	74.4	74.3	74.4	77.0	76.6	76.4	80.1	79.5	80.4	77.4	76.7	76.6
O	25.6	25.7	25.6	23.0	23.4	23.6	19.9	20.1	19.7	22.6	23.3	23.4

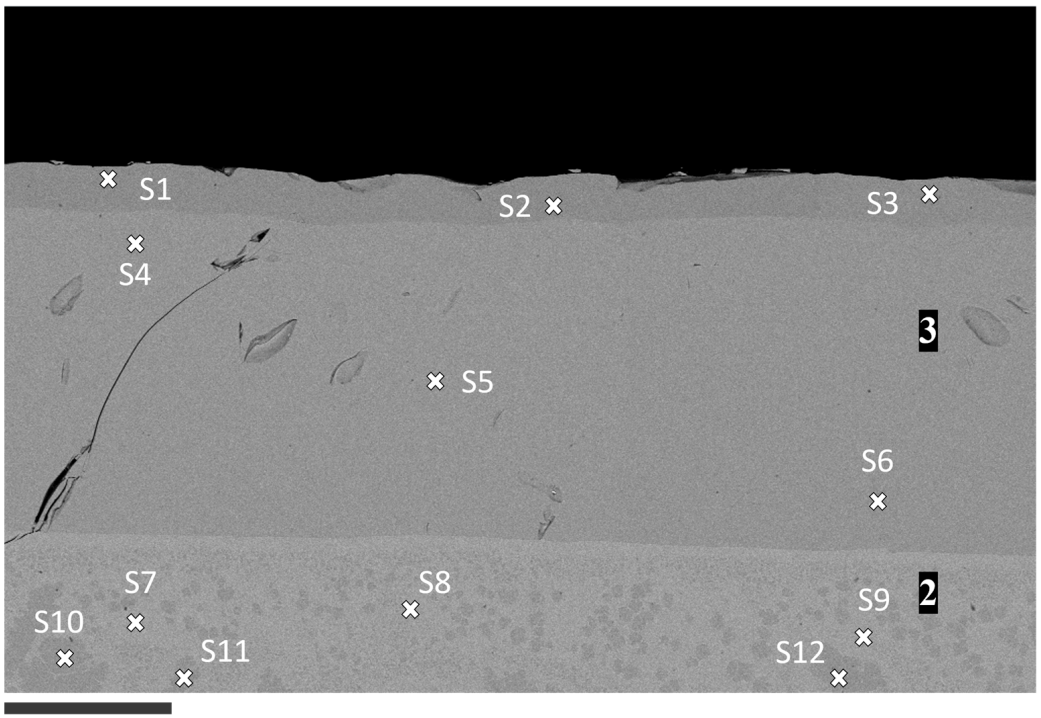

Figure 5. FESEM-EDS spectra for the iron oxide surface layers 2 and 3 of steel grade A oxidized in H_2–air atmosphere at 1230 °C (556× magnification). Identified oxide phases: S1–S3 hematite; S4–S6 magnetite; S7–S9 wüstite (light grey); S10–S12 magnetite precipitates (dark grey) mixed in wüstite. The scale bar is 100 μm.

The majority of layer 3 (S4–S6) has the same Fe:O ratio as the precipitates inside layer 2 (S10–S12); hence, both were identified as magnetite. The thin hematite layer on the surface was not always a smooth layer as shown in Figure 5, but sometimes appeared as pointed stripes. Hematite also occasionally extended deeper into the magnetite layer through cracks and voids.

3.3. Adhesion of the Steel–Scale Interface

Hultquist et al. [31] have stated that when the oxidation of metals occurs on the oxide–gas interface because of metal cation diffusion, scales tend to have poor adhesion to the metal substrate. When oxidation occurs mainly on the metal–oxide interface due to migration of oxygen anions, scales tend to crack due to tensile stress and the release of compressive stress. For cracks, voids and cavities to heal, both anion and cation diffusion to that area must occur. When anion and cation transport are well balanced, the scales tend to be thick, dense and adherent.

Another explanation for enhanced adhesion of the steel–scale interface in moist gas atmospheres is increased plasticity of the iron oxide caused by incorporation of hydrogen into the oxide lattice [13]. While it is established that water vapor can increase scale adhesion when compared to dry conditions, little research exists on whether the content of the water vapor influences the degree of oxide scale adhesion in moist gas atmospheres. Because the water vapor content in potential future reheating conditions is significantly elevated, it is of interest whether it will also influence the adhesion of the oxide scale. As previously stated, high scale adhesion can lead to descaling issues and potential surface defects during the hot-rolling stage. In this study, the adhesion of the formed oxide scale was estimated based on FESEM images from the steel–oxide interface. The adhesion of the interface was estimated by observing points of connection between the oxide and steel, the formation of a clear cooling gap and potential remnants of oxide on the surface of steel.

The steel–scale interface after oxidation at 1230 °C in different gas atmospheres is depicted in Figure 6. This temperature was selected for highlighting the differences between

gas atmospheres due to it being closest to the generally reported maximum reheating temperature of around 1200–1250 °C. By nature, the structure and adhesion of the steel–scale interface is very heterogenous. Therefore, several images were taken from the interface with a 300× magnification. Images that were considered representative of the interface as a whole were selected to be included in Figure 6.

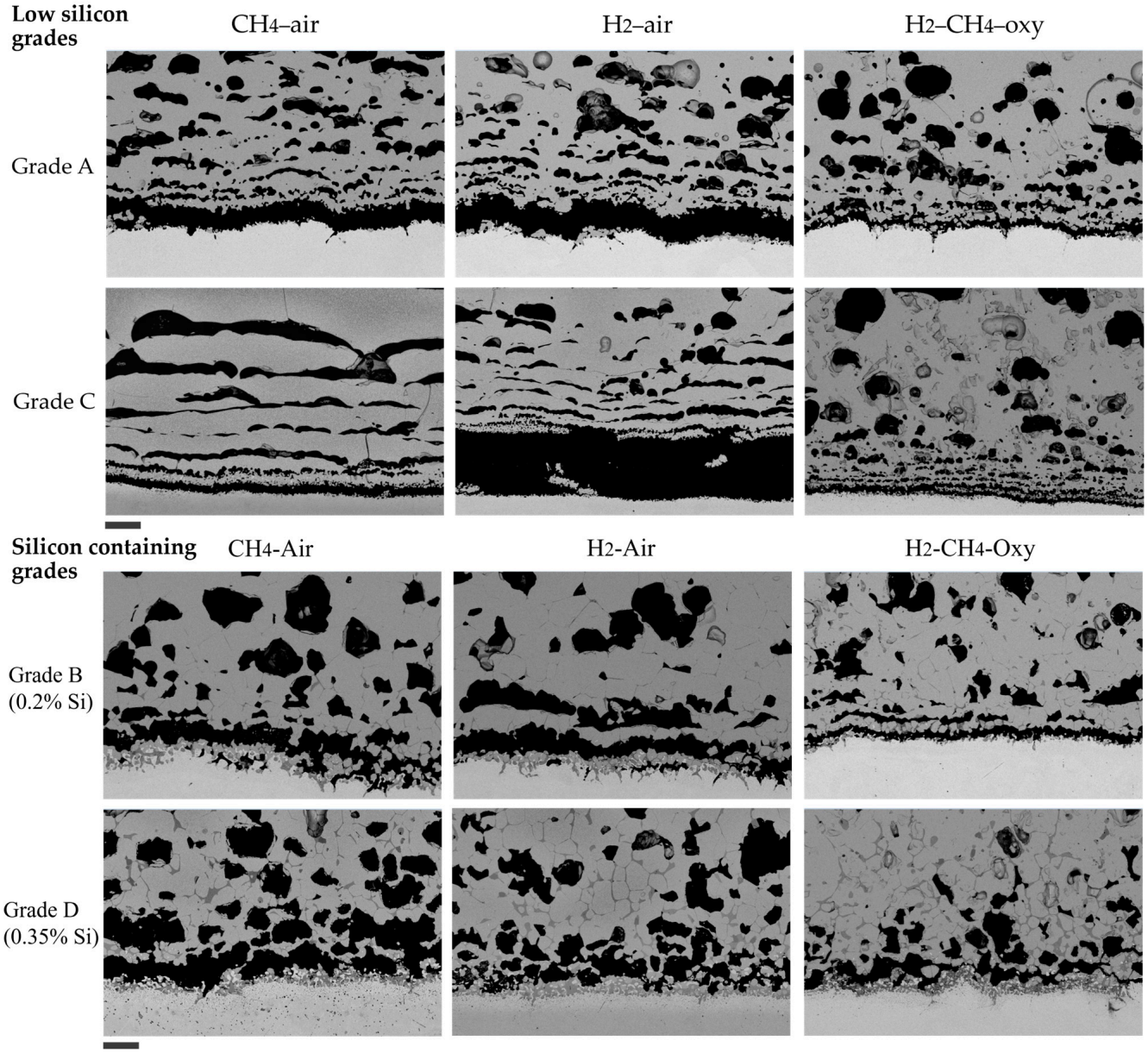

Figure 6. The steel–oxide interface (300× magnification) of all steel grades after oxidation at 1230 °C in various gas atmospheres. The scale bars are 100 μm.

In general, very few differences between the gas atmospheres were seen regarding the adhesion of the interface. For all the low-silicon steel grades, a clear gap formed between the steel and the oxide scale. It is considered that this gap was formed during the cooling stage as a result of differences in the thermal expansion rate of the oxide and steel. For the low-silicon grades, the gap at the interface was the largest for H_2–air; however, a similar result was not observed at 1150 °C or 1300 °C, so it could have been simply caused by variance. At these temperatures, few differences were found between the gas atmospheres.

In general, no clear improvement in the adhesion of the oxide scale could be seen even with significantly elevated water vapor contents in the gas atmosphere.

For the silicon-containing steel grades B and D, the adhesion of the steel–scale interface was clearly higher compared to the low-silicon grades. This is caused by the formation of the liquid FeO–Fe_2SiO_4 above 1173 °C; however, again no clear differences were found between the gas atmospheres regarding adhesion.

An interesting observation though was the change in pore structure in different gas atmospheres. In the CH_4–air gas atmosphere, the pore shape was generally flatter in the horizontal direction, especially for grades A and C. In H_2–air and especially in CH_4–H_2–oxy, on the other hand, the pore shape became more rounded. Macroporosity also seemed to be higher in the oxide scale in gas atmospheres with more water vapor. This effect, however, could simply be caused by a higher oxidation rate in these gas atmospheres. A more detailed analysis of the pore structural changes caused by differences in the gas atmosphere requires a separate study.

Luzzo et al. [27] have previously studied the oxidation of steel and descaling ability in natural gas and compared it to a 50:50 H_2–natural gas split. The authors found no difference in the descaling ability. The observations of this study are aligned with those of Luzzo et al. We did not find any visible sign of increased adhesion at the metal–scale interface in different gas atmospheres after cooling in ambient air. The cooling in our tests can be considered rapid, which causes a significant thermal stress on the samples. It is possible that more subtle differences between the gas atmospheres could possibly be seen with slower cooling rates.

It is hypothesized that moisture improves the plasticity and therefore also the adhesion of iron oxides compared to dry conditions during the growth phase as reported in previous studies, which prevents the oxide from spalling and allows for continuous flow of iron cations. However, if the moisture content is at a sufficient level to prevent spalling, there may not be significant differences between gas atmospheres with varying moisture contents regarding the final adhesion of the steel–scale interface. Based on the observations of this study, a change in reheating conditions to a carbon-free gas atmosphere or the utilization of the oxyfuel process are not expected to cause significant problems during the descaling process.

Two factors that did have a clear effect on the adhesion of the steel–scale interface were the silicon content of the steel and temperature. The steel–scale interfaces of different steel grades oxidized in H_2–air test temperatures are portrayed in Figure 7. As can be seen in the figure, temperature did not have an equally strong influence on adhesion for low-silicon steel grades, although there were some minor signs of entanglement between the oxide and the steel at 1300 °C. The adherence for the silicon containing grades on the other hand gets progressively stronger as temperature increases. The liquid eutectic phase penetrates the steel substrate, creating an entanglement of Fe, FeO and Fe_2SiO_4. Especially at 1300 °C, a clear boundary between the steel and oxide can no longer be seen, and instead, solid steel is mixed in the oxide layer. This entanglement was strong enough to prevent any gap formation during the cooling phase.

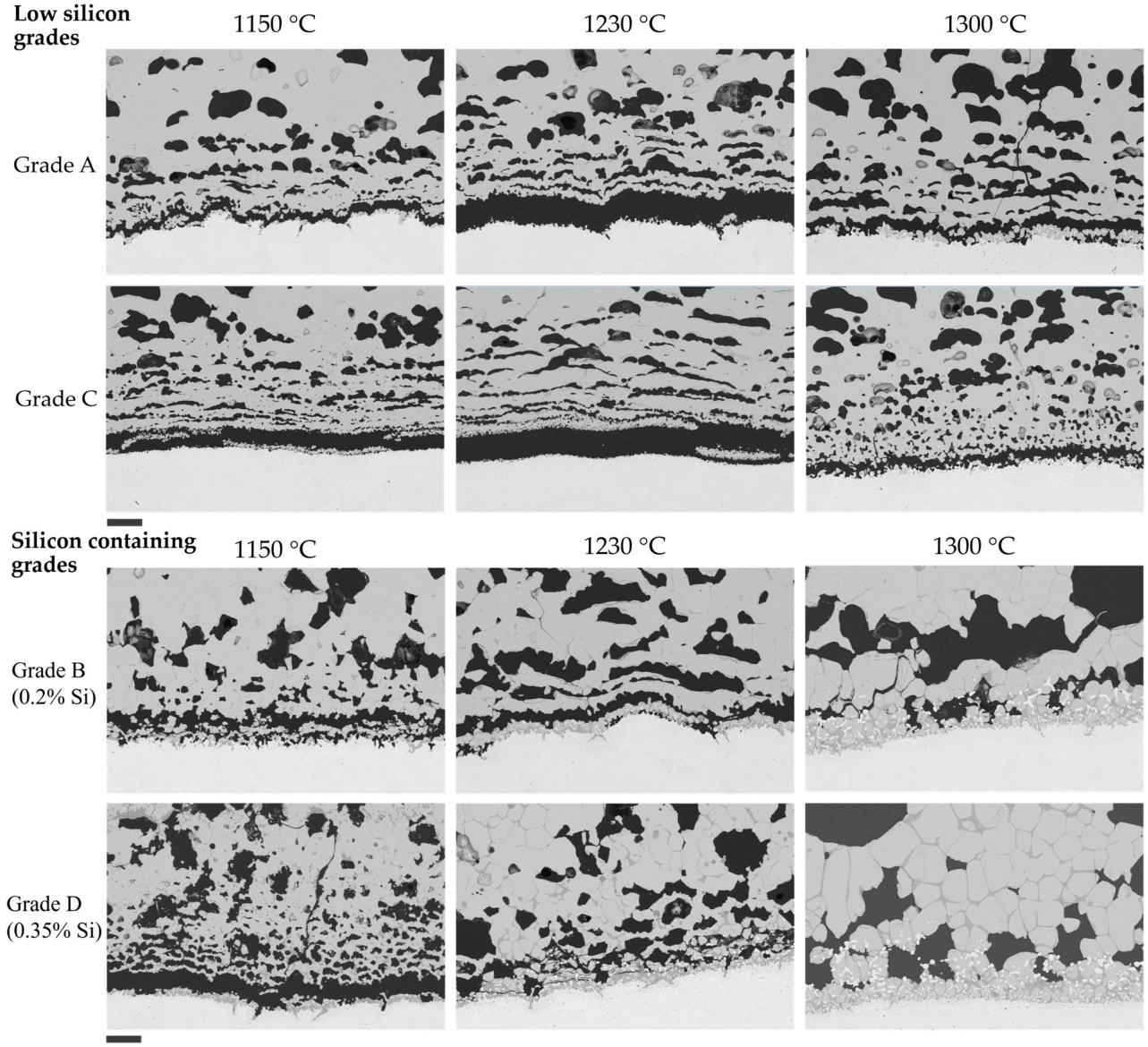

Figure 7. Steel–scale interface (300× magnification) for samples oxidized in H_2–air gas atmosphere at temperatures of 1150, 1230 and 1300 °C. The scale bars are 100 μm.

3.4. Dynamic Tests in CH_4–Air and H_2–Air

Dynamic tests were performed using a two-stage heating program with CH_4 and H_2 as fuel gases in a sequential manner. During the 250 min long oxidation period, the fuel gas changed after a 100 min oxidation in the first gas atmosphere, which was followed by a 150 min oxidation period in the second gas atmosphere. The temperature in the furnace at the 100 min mark was roughly 873 °C.

Points of interest to be analyzed were the following: (1) how is the total amount of oxide formation affected by the order of the fuel gases; (2) how does the oxidation rate between the gas atmospheres differ depending on the temperature; (3) and finally to analyze whether the adhesion of the steel–scale interface is affected by the gas atmospheres in dynamic temperature conditions. The overall structure of the oxide scale formed after a dynamic temperature profile can also be considered to better resemble the oxide scale formed in an industrial reheating furnace.

Dynamic tests were only performed for steel grades B and D. Steel grade B was low in silicon and grade D contained more alloying elements that affect the oxidation process,

namely silicon (0.36 wt%) and aluminum (<1 wt%). The dynamic TGA mass change curves in dynamic conditions are presented in Figure 8.

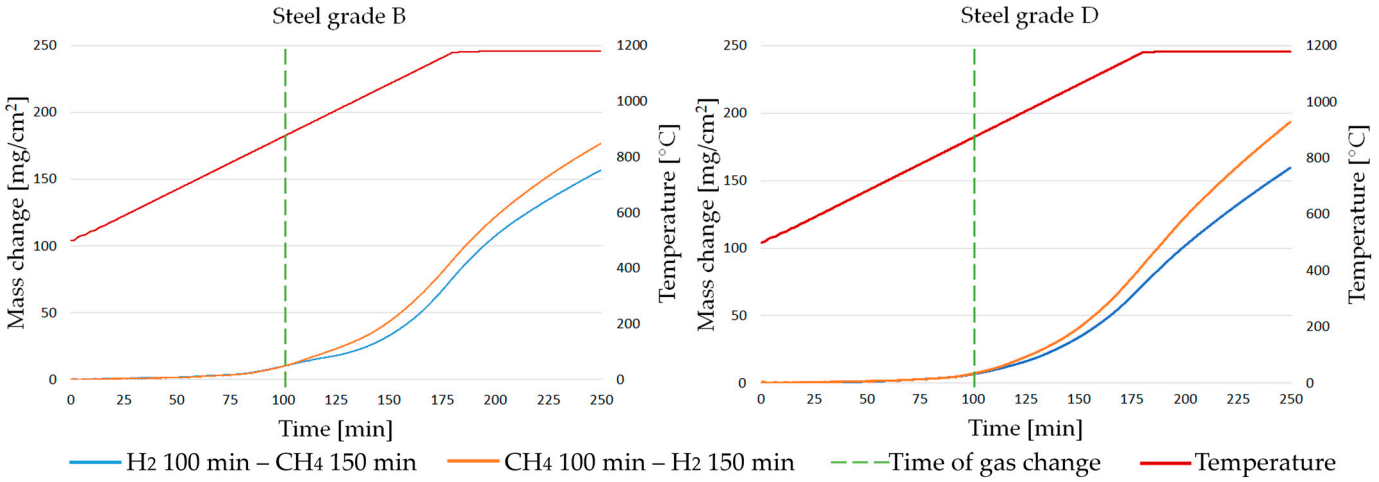

Figure 8. TGA mass change curves in dynamic conditions for steel grades B and D. The red curve on the secondary *y*-axis indicates the measured temperature inside the furnace.

When H_2 was introduced during the first 100 min and CH_4 after, the total mass growth was reduced by 12.8% for grade B and by 21.3% for steel grade D when compared to the opposite case of CH_4–H_2. Hence, in a hypothetical reheating scenario where a two-stage heating system could be implemented, for the purposes of minimizing scaling losses, the water vapor-rich gas atmosphere, such as H_2–air, should be implemented first, as the majority of oxide formation occurs at high temperatures.

An overall image of the formed oxide scales in dynamic temperature conditions is depicted in Figure 9. As can been seen from Figure 9, both the heating method (dynamic vs. isothermal) and the order of the gas atmospheres had a notable impact on the pore structures formed. In contrast to the isothermal tests, pores formed in dynamic conditions were elongated in the vertical direction in the upper part of the oxide scale. This effect was independent of the order of the gas atmospheres; however, when H_2–air was introduced first, the total porosity in the upper oxide layer was visibly higher for both steel grades. This effect was observable even though only a small portion of the oxidation occurred before the 100 min mark (873 °C) when the gas switch occurred.

In the lower part of the oxide layer, there was an observable change in pore shape similar to the isothermal tests: when H_2–air was introduced in the latter stage, the pore shapes in the lower oxide layer appeared to be more rounded compared to those formed in CH_4–air. A close-up image of the steel–scale interface after dynamic testing is depicted in Figure 10.

Regarding the adhesion of the steel–scale interface in dynamic conditions, the order of using H_2–air and CH_4–air did not have any observable influence. As could be expected, more oxide was attached to the steel substrate for grade D, which contained both Si and Al. From the FESEM images, it can be deduced that also in dynamic temperature conditions, any possible effect of the gas atmosphere on the adhesion of the steel–scale interface is likely to be overshadowed by the influence of alloying elements in the steel.

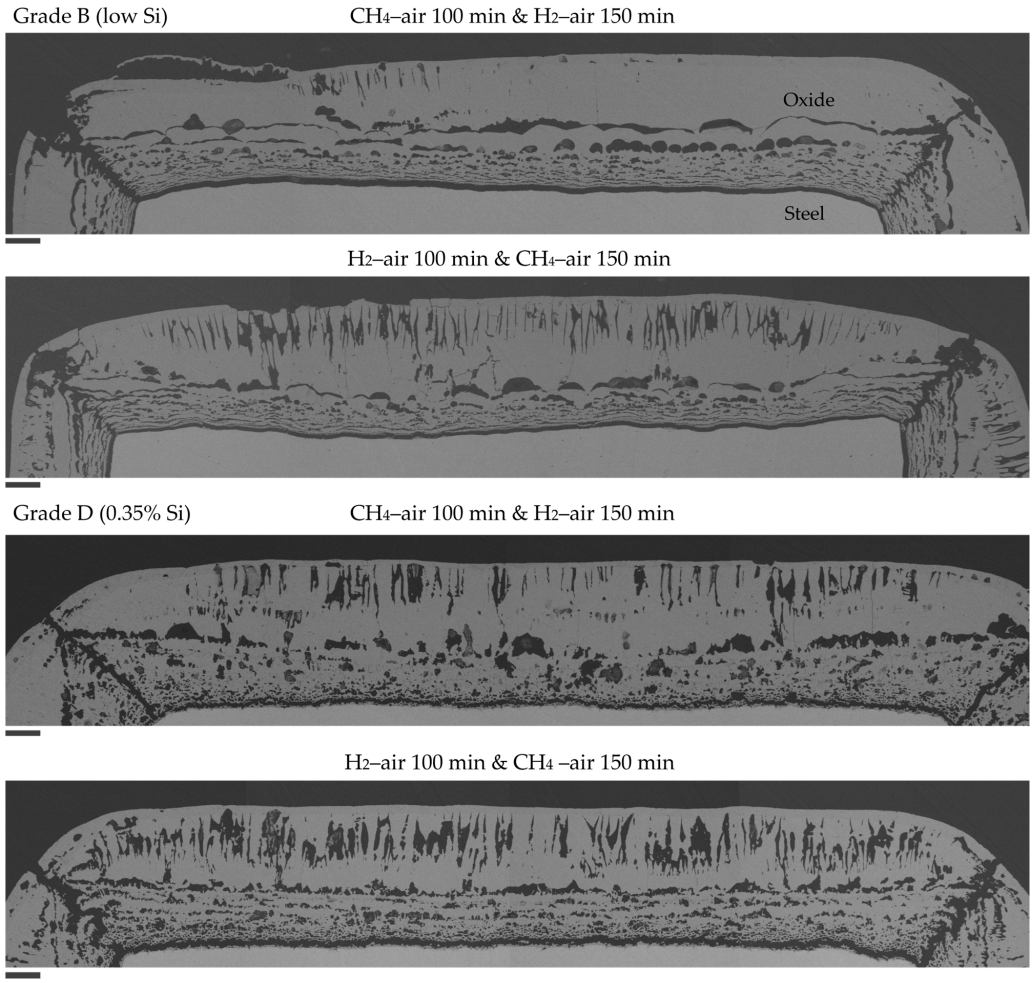

Figure 9. An overall image of the oxide scales formed on steel grades B and D during a two-stage heating scenario in dynamic temperature conditions. The scale bars are 400 μm.

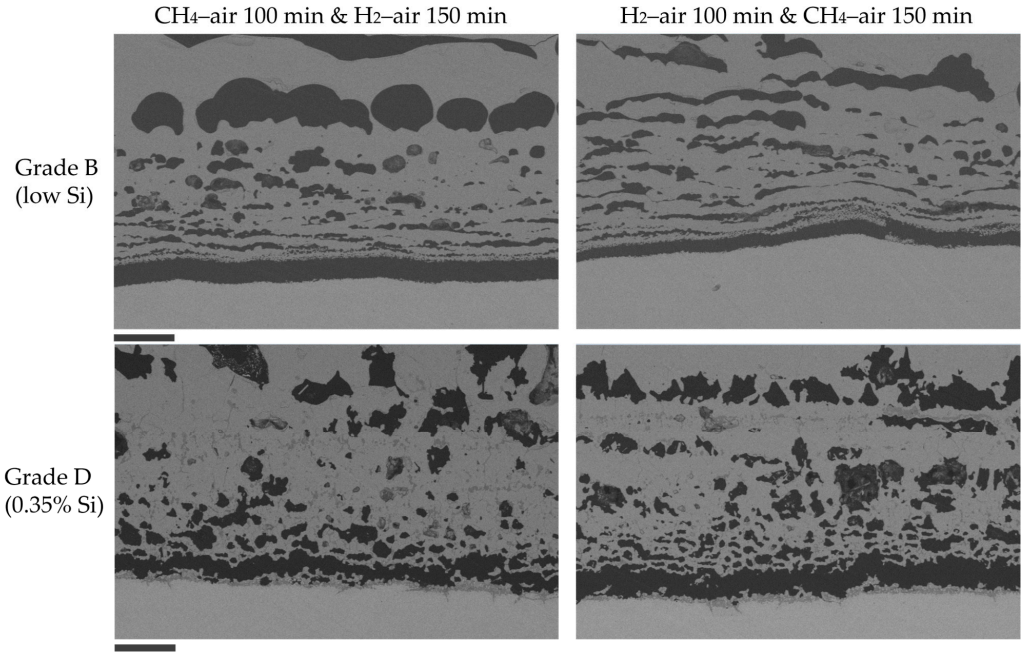

Figure 10. Adhesion of the steel–scale interface (200× magnification). The scale bars are 200 μm.

4. Conclusions

In this study, the effects of four current and novel reheating gas atmospheres on oxide formation on four low-carbon steel grades were studied. Based on the results obtained, the following conclusions are drawn:

1. Oxide formation increased in all four steel grades in the novel gas atmospheres H_2–air and CH_4–H_2–oxyfuel when compared to the current practices of methane–air and coke oven gas–air. From a scaling loss standpoint, the transition to H_2 burn in air produced a more moderate increase, whereas the oxyfuel scenario was by far the most oxidizing. The total oxidation in the four tested gas atmospheres correlated with the water vapor content.
2. Large differences were found between individual steel grades regarding the increase in oxidation in the novel gas atmospheres. In other words, some grades may be better suited for H_2 or oxyfuel reheating gas atmospheres than others.
3. No significant differences were observed between the gas atmospheres regarding the adhesion of the steel–scale interface after cooling in ambient air. Hence, the novel reheating gas atmospheres are not expected to cause significant descaling problems.
4. The adhesion of the steel–scale interface was mainly determined by the silicon content of the steel and temperature. For the silicon-containing grades, the test temperature had a large influence on adhesion due to the formation of a liquid FeO–Fe_2SiO_4 phase, which penetrated the oxide and steel creating a strong entanglement. Temperature, however, had little influence on the low-silicon steel grades with regards to the adhesion of the metal–scale interface.
5. The increase in water vapor in the novel gas atmospheres did seem to have an influence on the porosity and pore shape of the iron oxides; however, a more detailed study is required on this topic.

Author Contributions: Conceptualization, J.H., S.A. and E.-P.H.; investigation, S.R., J.H. and S.A.; validation, J.H.; writing—original draft preparation, J.H.; writing—review and editing, S.A., E.-P.H. and T.F.; visualization, J.H.; supervision, S.A., E.-P.H. and T.F. All authors have read and agreed to the published version of the manuscript.

Funding: This research is a part of the Business Finland funded FFS (Towards Fossil-Free Steel) research project, which was launched in the summer of 2021.

Data Availability Statement: Dataset is contained within the article. The original contributions presented in the study are included in the article, further inquiries can be directed to the corresponding author.

Acknowledgments: SSAB Europe Raahe is credited for coordinating the research and providing feedback.

Conflicts of Interest: The authors declare no conflicts of interest.

References

1. Rogelj, J.; Shindell, D.; Jiang, K.; Fifita, S.; Forster, P.; Ginzburg, V.; Handa, C.; Haroon, K.; Kobayashi, S.; Kriegler, E.; et al. Mitigation Pathways Compatible with 1.5 °C in the Context of Sustainable Development. In *IPCC Special Report on Global Warming of 1.5 °C*; Cambridge University Press: Cambridge, UK, 2018; Chapter 2.
2. Rissman, J.; Bataille, C.; Masanet, E.; Aden, N.; Morrow, W.R.; Zhou, N.; Elliott, N.; Dell, R.; Heeren, N.; Huckestein, B.; et al. Technologies and Policies to Decarbonize Global Industry: Review and Assessment of Mitigation Drivers through 2070. *Appl. Energy* **2020**, *266*, 114848. [CrossRef]
3. Ginzburg, V.B. *Steel-Rolling Technology: Theory and Practice*, 1st ed.; CRC Press: Boca Raton, FL, USA, 1989.
4. Young, D.J. *High Temperature Oxidation and Corrosion of Metals*, 2nd ed.; Elsevier: Amsterdam, The Netherlands, 2016.
5. Fukagawa, T.; Okada, H.; Maehara, Y. Mechanism of Red Scale Defect Formation in Si-Added Hot-Rolled Steel Sheets. *ISIJ Int.* **1994**, *34*, 906–911. [CrossRef]
6. Mayr, B.; Prieler, R.; Demuth, M.; Moderer, L.; Hochenauer, C. CFD Modelling and Performance Increase of a Pusher Type Reheating Furnace Using Oxy-Fuel Burners. *Energy Procedia* **2017**, *120*, 462–468. [CrossRef]
7. Hu, Y.; Tan, C.K.; Niska, J.; Chowdhury, J.I.; Balta-Ozkan, N.; Varga, L.; Roach, P.A.; Wang, C. Modelling and Simulation of Steel Reheating Processes under Oxy-Fuel Combustion Conditions—Technical and Environmental Perspectives. *Energy* **2019**, *185*, 730–743. [CrossRef]

8. Schmitz, N.; Sankowski, L.; Kaiser, F.; Schwotzer, C.; Echterhof, T.; Pfeifer, H. Towards CO_2-Neutral Process Heat Generation for Continuous Reheating Furnaces in Steel Hot Rolling Mills—A Case Study. *Energy* **2021**, *224*, 120155. [CrossRef]
9. Saunders, S.R.J.; Monteiro, M.; Rizzo, F. The Oxidation Behaviour of Metals and Alloys at High Temperatures in Atmospheres Containing Water Vapour: A Review. *Prog. Mater Sci.* **2008**, *53*, 775–837. [CrossRef]
10. Rahmel, A.; Tobolski, J. Einfluss von Wasserdampf Und Kohlendioxyd Auf Die Oxydation von Eisen in Sauerstoff Bei Hohen Temperaturen. *Corros. Sci.* **1965**, *5*, 333–340. [CrossRef]
11. Chen, R.Y.; Yuen, W.Y.D. Effects of the Presence of Water Vapour on the Oxidation Behaviour of Low Carbon-Low Silicon Steel in 1%O_2-N_2 at 1073 K. *Oxid. Met.* **2013**, *79*, 655–678. [CrossRef]
12. Lee, V.H.J.; Gleeson, B.; Young, D.J. Scaling of Carbon Steel in Simulated Reheat Furnace Atmospheres. *Oxid. Met.* **2005**, *63*, 15–31. [CrossRef]
13. Tuck, C.W.; Odgers, M.; Sachs, K. The Oxidation of Iron at 950 °C in Oxygen/Water Vapour Mixtures. *Corros. Sci.* **1969**, *9*, 271–280. [CrossRef]
14. Yun, J.Y.; Ha, S.A.; Kang, C.Y.; Wang, J.P. Oxidation Behavior of Low Carbon Steel at Elevated Temperature in Oxygen and Water Vapor. *Steel. Res. Int.* **2013**, *84*, 1252–1257. [CrossRef]
15. Gaiser, G.; Presoly, P.; Bernhard, C. High-Temperature Oxidation of Steel under Linear Flow Rates of Air and Water Vapor—An Experimental Determined Set of Data. *Metals* **2023**, *13*, 892. [CrossRef]
16. Arreola-Villa, S.A.; Vergara-Hernández, H.J.; Solorio-Diáz, G.; Pérez-Alvarado, A.; Vázquez-Gómez, O.; Chávez-Campos, G.M. Kinetic Study of Oxide Growth at High Temperature in Low Carbon Steel. *Metals* **2022**, *12*, 147. [CrossRef]
17. Osei, R.; Lekakh, S.; O'Malley, R. Effect of Al Additions on Scale Structure and Oxidation Kinetics of 430-Ferritic Stainless Steel Reheated in a Combustion Atmosphere. *Metall. Mater. Trans. B* **2021**, *52*, 3423–3438. [CrossRef]
18. Cheng, L.; Sun, B.; Du, C.; Gao, W.; Cao, G. High-Temperature Oxidation Behavior of Fe–10Cr Steel under Different Atmospheres. *Materials* **2021**, *14*, 3453. [CrossRef] [PubMed]
19. Haapakangas, J.; Suopajärvi, H.; Iljana, M.; Kemppainen, A.; Mattila, O.; Heikkinen, E.P.; Samuelsson, C.; Fabritius, T. Coke Reactivity in Simulated Blast Furnace Shaft Conditions. *Metall. Mater. Trans. B* **2016**, *47*, 2357–2370. [CrossRef]
20. Faramawy, S.; Zaki, T.; Sakr, A.A.E. Natural Gas Origin, Composition, and Processing: A Review. *J. Nat. Gas Sci. Eng.* **2016**, *34*, 34–54. [CrossRef]
21. Zhang, H.; Yu, L.; Liu, T.; Ni, H.; Li, Y.; Chen, Z.; Yang, Y. Optimizing the Preheating Temperature of Hot Rolled Slab from the Perspective of the Oxidation Kinetic. *J. Mater. Res. Technol.* **2020**, *9*, 12501–12511. [CrossRef]
22. Chang, Y.N.; Wei, F.I. High Temperature Oxidation of Low Alloy Steels. *J. Mater. Sci.* **1989**, *24*, 14–22. [CrossRef]
23. Alaoui Mouayd, A.; Koltsov, A.; Sutter, E.; Tribollet, B. Effect of Silicon Content in Steel and Oxidation Temperature on Scale Growth and Morphology. *Mater. Chem. Phys.* **2014**, *143*, 996–1004. [CrossRef]
24. Suarez, L.; Schneider, J.; Houbaert, Y. High-Temperature Oxidation of Fe-Si Alloys in the Temperature Range 900–1250 °C. *Defect Diffus. Forum* **2008**, *273–276*, 661–666. [CrossRef]
25. Yuan, Q.; Xu, G.; Zhou, M.; He, B. The Effect of the Si Content on the Morphology and Amount of Fe_2SiO_4 in Low Carbon Steels. *Metals* **2016**, *6*, 94. [CrossRef]
26. Mikl, G.; Höfler, T.; Gierl-Mayer, C.; Danninger, H.; Linder, B.; Angeli, G. Scaling Behaviour of Si-Alloyed Steel Slabs under Reheating Conditions. *J. Cast. Mater. Eng.* **2021**, *5*, 71–74. [CrossRef]
27. Luzzo, I.; Cirilli, F.; Jochler, G.; Gambato, A.; Longhi, J.; Rampinini, G. Feasibility Study for the Utilization of Natural Gas and Hydrogen Blends on Industrial Furnaces. *Mater. Tech.* **2021**, *109*, 306. [CrossRef]
28. Chen, R.Y.; Yuen, W.Y.D. Review of the High-Temperature Oxidation of Iron and Carbon Steels in Air or Oxygen. *Oxid. Met.* **2003**, *59*, 433–468. [CrossRef]
29. Raman, R.K.S.; Gleeson, B.; Young, D.J. Laser Raman Spectroscopy: A Technique for Rapid Characterisation of Oxide Scale Layers. *Mater. Sci. Technol.* **1998**, *14*, 373–376. [CrossRef]
30. Yuan, Q.; Xu, G.; He, B.; Zhou, M.X.; Hu, H.J. A Method to Reduce the Oxide Scale of Silicon-Containing Steels by Adjusting the Heating Route. *Trans. Indian Inst. Met.* **2018**, *71*, 677–684. [CrossRef]
31. Hultquist, G.; Tveten, B.; Hörnlund, E.; Limbäck, M.; Haugsrud, R. Self-Repairing Metal Oxides. *Oxid. Met.* **2001**, *56*, 313–346. [CrossRef]

Disclaimer/Publisher's Note: The statements, opinions and data contained in all publications are solely those of the individual author(s) and contributor(s) and not of MDPI and/or the editor(s). MDPI and/or the editor(s) disclaim responsibility for any injury to people or property resulting from any ideas, methods, instructions or products referred to in the content.